FORM TI-12
8/94

WAPD-T-3110

CONF-9605346--

THE HYDROGEN EMBRITTLEMENT OF Ni-Cr-Fe ALLOYS

D. M. Symons

DE-AC11-93PN38195

BETTIS ATOMIC POWER LABORATORY WEST MIFFLIN, PENNSYLVANIA 15122-0079

Operated for the U.S. Department of Energy
by WESTINGHOUSE ELECTRIC CORPORATION

DISCLAIMER

Portions of this document may be illegible in electronic image products. Images are produced from the best available original document.

Hydrogen Embrittlement of Ni-Cr-Fe Alloys

D.M. Symons

ABSTRACT

Stress corrosion cracking (SCC) of Alloy 600 and Alloy 690 in elevated temperature water has been well documented((1),(2),(3),(4)). When tested in low-temperature hydrogenated water, Alloy 690 (30% Cr) has shown a five-fold decrease in its fracture toughness while Alloy 600 (15% Cr) shows no effect of environment on its fracture toughness behavior(5). It has been proposed that the SCC of nickel-based alloys in low-temperature hydrogenated water is due to hydrogen embrittlement((6),(7)). The purpose of this work was to investigate the role of chromium on hydrogen embrittlement of Ni-Cr-Fe alloys and thus develop a better understanding of the low-temperature SCC phenomenon. The effect of chromium on the hydrogen embrittlement was examined using tensile tests followed by material evaluation via scanning electron microscopy and light optical microscopy. Four alloys were prepared with chromium contents ranging from 6 wt. percent to 35 wt. percent. In the noncharged condition, ductility, as measured by the percent elongation or reduction in area, increased as the alloy chromium content increased. Hydrogen appeared to have only minor effects on the mechanical properties of the low chromium alloys. The addition of hydrogen had a marked effect on the ductility of the higher chromium alloys. In the 26% chromium alloy, the elongation to failure was reduced from 53% to 14% with a change in fracture mode from

ductile dimple to intergranular failure. A maximum in embrittlement was observed in the 26% Cr alloy. The maximum in embrittlement coincided with the minimum in stacking- fault energy. The correlation of hydrogen embrittlement with stacking-fault energy has been observed previously in stainless steels (8). It is proposed that the increased hydrogen embrittlement in the high-chromium alloys is due to increased slip planarity caused by the low stacking-fault energy. Slip planarity did not appear to affect the fracture of the noncharged specimens.

INTRODUCTION

There appear to be two environmentally enhanced cracking phenomena associated with nickel-base alloys in a hydrogenated water environment. The high-temperature stress corrosion cracking behavior of Ni-XCr-9Fe alloys, where Cr is between 15% and 30% Cr, in high purity water has been well documented((1),(2),(3),(4)). The low-temperature stress corrosion cracking of the solid solution alloys with the composition of Ni-XCr-9Fe in hydrogenated water has recently been reported(5). The first phenomenon, high-temperature SCC, has been observed between 250°C and 360°C. This phenomenon is characterized by a time to incubate the crack followed by a relatively low crack growth rate, on the order of 0.05 mm/day in 360°C deaerated hydrogenated water depending on load. The high-Cr alloys are significantly more resistant to high-temperature pure-water SCC than the lower-Cr alloys. The second phenomenon, low-temperature cracking, occurs at temperatures below 150°C. This phenomenon is characterized by a decrease in the fracture toughness of the material or rapid stable crack growth. It has been shown that

solid solution strengthened Alloy 690 (~30% Cr) is susceptible to this low-temperature embrittlement phenomenon in deaerated hydrogenated pure water while Alloy 600 (~15% Cr) is not(5). Most tests for low-temperature SCC have been performed on Alloy X-750(15% Cr), a high-strength gamma-prime-strengthened material that shows very localized deformation(9). It was shown that the low-temperature SCC is hydrogen embrittlement ((6),(7)). That work demonstrated that fracture behavior was sensitive to phosphorus segregation at the grain boundaries, and that the crack growth rate was as high as 0.03 mm/s, a rate higher than can be modeled by anodic dissolution(6).

The primary difference between Alloy 600 and Alloy 690 is the amount of chromium in the alloys, 15 wt. percent and 30 wt. percent, respectively. This difference in chromium content may alter the deformation behavior (10), which, in turn, may change the material susceptibility to hydrogen embrittlement. In stainless steels increased slip planarity results in increased susceptibility to hydrogen embrittlement(8). The slip mode in these alloys is partially controlled by the stacking fault energy, which is dependent on the chromium concentration. It has also been proposed that the slip planarity may control the hydrogen embrittlement phenomenon in the nickel-base alloys(8)(11). In the nickel-chromium system, there appears to be a minimum in stacking-fault energy at approximately 25% chromium (10)(12). Therefore, if stacking fault energy is a controlling factor in the hydrogen embrittlement of these alloys, a maximum in embrittlement is expected at around 25%.

It was the objective of this work to understand the effect of chromium on hydrogen embrittlement in Ni-Cr-Fe alloys at ambient temperature. These results may then be compared with the low-temperature SCC behavior. The work reported herein utilized tensile specimens with Cr contents ranging from 6% to 35%. By performing tensile tests on materials in the as-received condition and the hydrogen charged condition it was possible to evaluate the degree of embrittlement as a function of alloy chromium content. A mechanism is proposed herein to describe the observed embrittlement phenomenon.

EXPERIMENTAL TECHNIQUES

Materials

The alloys were produced using a nonconsumable arc melting process in an inert (argon) atmosphere that produced 75 mm diameter buttons. All raw materials used in the initial melt were greater than 99.9% pure, the nickel being 99.99%. The materials were triple melted per the following procedure to assure a uniform composition.

1st melt.	Preweigh raw materials and section into small pieces. Melt into buttons at 800 amps.
2nd melt	Clean buttons in acid. Cut into small pieces, remelt at 800 amps.
3rd melt	Clean buttons in acid. Cut into small pieces, remelt at 800 amps. Flip button and remelt to homogenize.

The buttons were then annealed at 1000°C and rolled for a single reduction of 30%. Two more rolling passes each with a 30% reduction and intermediate anneal at 1100°C were performed on the buttons. This resulted in four plates of the alloys with an average thickness of 3.5 mm. A final anneal at 1065°C was followed by an air cool. The chemical compositions of the heats are presented in Table I. The titanium was added to increase hot workability.

TABLE I: CHEMISTRY OF Ni-XCr-8Fe Heats

Heat	%Ni	%Cr	%Fe	%Ti	%C	S (ppm)	P (ppm)
1	85.3	6.1	8.4	0.21	0.025	<25	<25
2	76.7	14.7	8.4	0.21	0.031	<25	<25
3	65.1	26.5	8.2	0.21	0.033	<25	<25
4	56.7	34.8	8.3	0.21	0.034	<25	<25

Flat uniaxial tensile specimens with a cross-sectional area of 3.2 mm x 1.27 mm and a gage length of 12.5 mm were machined from the plates with the gage length parallel to the rolling axis. Two specimens from each alloy were hydrogen charged.

The hydrogen charging was performed in a high-pressure hydrogen autoclave. The specimens were cleaned in acetone then alcohol rinsed prior to insertion into the autoclave. The hydrogen gas entering the autoclave was purified by running the gas line through a liquid nitrogen bath that condensed impurities from the hydrogen. The charging was accomplished at a hydrogen pressure of 34 MPa hydrogen at

285°C for six weeks to assure uniform hydrogen concentration. According to Crank (13), the time needed to achieve a uniform hydrogen concentration is determined when the dimensionless parameter, Dt/l^2 (diffusivity multiplied by time and divided by one-half the thickness) is equal to 1.5. The diffusivity of hydrogen in Alloy 600 is given by(14):

$$D_H = 0.049 \exp\left[\frac{-42{,}400}{RT}\right] \quad (1)$$

where R is in J/mol, T is in Kelvin, and D_H is in cm^2/s. For this thickness, the minimum time required is calculated to be three hours as compared to the six weeks used in this experiment. The hydrogen concentration was measured after hydrogen charging using a LECO hydrogen analyzer model RH404. The measured hydrogen concentrations from the gas phase hydrogen charging are displayed in Table II.

Table II: The Concentration of Hydrogen in the Hydrogen Charged Tensile Specimens

Alloy	% Cr	Hydrogen (wppm)
1	6.1	37
2	14.7	36
3	26.5	55
4	34.8	99

Four tensile specimens from each alloy were tested: two in the as received condition and two in the hydrogen charged condition. All tensile specimens were

tested at 25°C at an initial strain rate of $4x10^{-4}s^{-1}$. An extensometer was used to measure the strain on all the specimens. The tests were analyzed to determine the percent reduction in area (% RA), the percent elongation (% El), the percent RA loss due to hydrogen, percent elongation loss, the yield strength, and the ultimate tensile strength. The percent RA loss and percent elongation loss are defined as:

$$\text{RA loss} = \left(1 - \frac{\text{RA of hydrogen charged specimen}}{\text{RA of noncharged specimen}}\right) * 100$$

$$\text{El loss} = \left(1 - \frac{\text{elongation of hydrogen charged specimen}}{\text{elongation of noncharged specimen}}\right) * 100$$

The fracture morphology was characterized by scanning electron microscopy (SEM) to determine the relationship between microstructure, fracture behavior, and fracture morphology.

RESULTS

Microstructural Characterization

The microstructure consisted of equiaxed grains, the average grain size ranged from 200 μm to 300 μm as shown for the Alloys 1 through 4 in Figures 1 through 4, respectively. All the alloys have small transgranular primary titanium carbides throughout the specimens. These carbides were aligned along the rolling direction. The grain boundaries were also partially covered with carbides on all the specimens. These intergranular carbides are expected to be chromium carbides(15)(16).

Mechanical Property Characterization

The results will be discussed in two parts. The first part will discuss the results of the testing of the noncharged specimens. The second part will discuss the results of the hydrogen charged specimens.

TABLE III: Tensile Properties of Experimental Alloys

Alloy	H charged	0.2% offset yield stress (MPa)	Ultimate Tensile Stress (MPa)	% Elongation	% RA	% Elongation loss	% RA loss
1	No	207	462	35	45	-	-
2	No	282	586	49	52	-	-
3	No	289	593	53	57	-	-
4	No	261	606	55	65	-	-
1	Yes	220	468	31	42	11	6
2	Yes	255	565	42	45	14	12
3	Yes	282	427	13.5	20	74	63
4	Yes	300	475	18	27	67	57

The effect of chromium on the tensile properties of Ni-XCr-8Fe alloys is shown in Table III. The alloy with the lowest chromium concentration has the lowest ductility. Increasing the percentage of chromium in the alloys increased the ductility in the noncharged condition, as is observed by the measurements of the elongation to failure and reduction in area. Scanning electron micrographs of the fracture surfaces show a change in fracture morphology as the Cr content is increased. In the alloys with the low chromium levels, classical ductile failure was observed. Dimples were observed in the center of the specimen and the final

fracture occurred by shear rupture at the surface as is shown in Figure 5. The voids appear to nucleate at the primary carbide particles, also shown in Figure 5. The size of the particles are similar to the titanium carbides and energy dispersive spectroscopy of the particles showed a higher titanium content that the matrix. In In the alloys with higher chromium contents, 26-35% Cr, the center of the specimen had approximately equal amounts of transgranular ductile dimple fracture and intergranular shear fracture, as shown in Fig. 6. The transgranular voids still formed at the primary carbides whereas it appears that intergranular failure is due to shear fracture along or very near the grain boundaries.

The strain hardening behavior was also affected by the chromium concentration. Figure 7 shows the strain hardening rate, $d\sigma/d\varepsilon$, as a function of the plastic strain. In all cases, the strain hardening shows a linear region at low strains. As the chromium content increases, the linear region exists to higher strains. Once the strain is past this linear strain hardening regime, the strain hardening decreases at a much higher rate in alloys with the lower chromium content. This suggests that cross-slip is easier at the lower chromium concentrations, consistent with the higher stacking fault energy of these alloys or possible short-range order in the high-chromium alloys(17)(18). With easier cross-slip, one would expect the strain-hardening rate to be lower. The final important parameter to measure is the yield strength. The 6% Cr alloy had the lowest yield strength. The other alloys, 15%Cr through 35% Cr, all had similar yield strengths.

The effect of Cr on the elongation to failure of the charged and noncharged specimens is shown in Figure 8. Hydrogen appears to have only minor effects on the mechanical properties and the fractographic features of the low-Cr alloys. However, there is slightly more embrittlement in the 15% chromium alloys compared to the 6% chromium alloy. This is also manifested in the fracture appearance. The 15% chromium alloy showed predominantly ductile dimple fracture, but transgranular facets were also present as shown in Figure 9. This is consistent with the observations by Thompson(11) on hydrogen charged Alloy 600 and Alloy 625.

The addition of hydrogen had a marked effect on the mechanical properties of the high Cr alloys. In the 26% Cr alloy, the elongation was reduced from 53% to 14%. In the 35% Cr alloy, the elongation was reduced from 55% to 18%. In both alloys, the ductile appearing fracture surface of the noncharged specimens changed to a much more brittle-appearing intergranular fracture morphology as shown in Figure 10 for the 26% Cr alloy. The intergranular faces are faceted in the hydrogen-charged case while for the noncharged specimens the intergranular faces appear to have failed by shear. The facets on the intergranular surface are consistent with slip band fracture. These intergranular facets are consistent with the slip bands observed on the surface of flat polished uniaxial tensile specimens strained to 1%, as shown in Figure 11.

DISCUSSION

The Effect of Chromium on the Fracture Behavior of Noncharged Specimens

The failure strain for the microvoid coalescence process is the sum of strain to initiate the voids and the strain to grow the voids. Since the low chromium alloys have less ductility than the higher chromium alloys, the addition of chromium must affect the microvoid nucleation and/or growth processes. Chromium may have two effects: 1) it may increase the strain required to initiate voids; and 2) it may increase the strain required for the voids to coalesce. Franklin et al.(19) observed that chromium in thoriated nickel increased the adhesion between thoria and the nickel matrix. Also, Gessinger and Fischmeister (20) showed that chromium increased the adhesion between alumina and an Fe-40Ni matrix. In the current system, chromium may increase the adhesion between the TiC and the matrix, thereby delaying the onset of void nucleation. It has also been shown that in Ni-Cr alloys, chromium may increase slip localization (17)(18). When slip is localized, the local strain rate in the slip band region increases which in turn increases void growth . Since the failure strain is much higher in the high-Cr alloys, it appears that void initiation occurs at higher strains with increasing chromium content and that increased slip planarity plays a secondary and counteracting role. In fact, the strain for the voids to initiate has increased to such an extent in the high-chromium alloys, that a second fracture mechanism becomes active, i.e., grain boundary fracture.

The Effect of Hydrogen on the Embrittlement of the Ni-Cr-Fe Alloys

Based on the results of this investigation, it is proposed that the high degree of hydrogen embrittlement in the high-chromium alloys is due to a more planar mode of slip in these alloys than in the low-Cr alloys. It has been shown that the slip mode strongly affects the susceptibility of FCC materials to SCC and hydrogen embrittlement (8). If the deformation is made more inhomogeneous and localized, materials become more susceptible to hydrogen embrittlement. In the Ni-Cr-Fe alloys, the deformation behavior can be made more planar by a reduction in stacking fault energy or short-range ordering, as discussed below.

One effect of alloying elements is to alter the stacking-fault energy, which in turn affects the mode of deformation. Homogeneous deformation is associated with large stacking-fault energies. It has been shown that increasing chromium concentration from 0% to 25% decreases the stacking fault energy(8)(12). Above 25% Cr, it appears that the stacking-fault energy may increase, see Figure 12. This is consistent with the change in strain-hardening behavior observed in these alloys as a function of chromium concentration. The loss in ductility appears to be inversely related to stacking-fault energy, as shown in Figure 13. The effect of iron on stacking-fault energy is not included in the calculation for stacking-fault energy. The effect of iron would be to displace all the numbers by a small additive term and would not affect the conclusions drawn from Figure 13 ((8),(12)).

In Ni-Cr alloys, it has been shown by specific heat measurements that between 10% Cr and 20% Cr, short range ordering occurs (21). It has also been shown by Akhtar and Teghtsoonian (22) that the deformation behavior of Ni-Cr alloys between 10% and 20% Cr is consistent with short range ordering. In Ni-Cr alloys, there is an intermetallic phase Ni_2Cr (Pt_2Mo type structure). When short-range ordering occurs in a material, glide becomes more planar. When the order is disrupted on a glide plane due to a dislocation passing through that plane, it becomes easier for dislocations to continue on that plane than to clear away the order on different planes. An example of short range order altering the slip planarity in nickel-base alloys and thereby increasing the susceptibility to hydrogen embrittlement has been observed for the nickel-base alloy C-276 (23). It should be noted though, that short range order has not been observed in Alloy 600 (24) though it is possible to have short range ordering in the high-Cr alloys. Furthermore, short range order is most important at low strains because at high strains the original nearest neighbors are disrupted.

The discussion thus far has focussed on the role of deformation on the hydrogen embrittlement of the solid-solution-strengthened alloys. There are other aspects of materials that may affect the embrittlement process, although for the Ni-Cr-Fe alloys, these appear to play only a secondary role. If either a decohesion mechanism or a void nucleation mechanism is important, then the yield strength would be important(25)(26). An increase in the yield stress will increase the local stress at a particle and allow decohesion to occur at a lower strain. In the Ni-Cr-Fe

alloys in this test program, the alloy with 15% Cr had a yield stress similar to that of the 26% and 35% Cr alloys, but these alloys showed much more embrittlement then the 15% Cr alloy. This suggests that yield strength did not play a major role in the embrittlement. Another important aspect of the embrittlement of materials due to hydrogen is the hydrogen concentration in the specimens. In Alloy X-750 it was shown that in a susceptible heat only 6 ppm hydrogen was sufficient for extensive embrittlement, while in a heat more resistant to hydrogen embrittlement 20 ppm hydrogen was necessary for extensive embrittlement (9). The change from slightly-embrittled to extensively-embrittled material was a step function at a critical hydrogen concentration. The alloys in this program were hydrogen charged at the same time in the same autoclave, though the hydrogen solubility, Sievert's Law, is different in the different alloys resulting in a range of hydrogen concentrations. Increasing the chromium content of the alloy increased the solubility of hydrogen at chromium contents greater than 15%. A comparison of the RA loss of the 6% Cr and 15% Cr alloys with the same hydrogen concentration, showed that the 15% Cr alloy was embrittled more. Also, the 26% Cr alloy with 55 ppm hydrogen was embrittled more than the 35% Cr alloy with 95 ppm hydrogen. This suggests that dissolved hydrogen, per se, plays a secondary role.

It has been proposed (8) that the intergranular fracture processes occur more readily in alloys that undergo planar slip. In the Ni-Cr-Fe alloy system, the increased slip planarity may increase the local grain boundary hydrogen concentration due to

dislocation transport of the hydrogen to the grain boundary (27). Also, the increased slip planarity may lead to local failure along slip bands near the grain boundary due to higher local stresses due to dislocation pile-ups. Hydrogen may increase the susceptibility for slip band fracture by weakening the bond strength of the atoms on the slip plane. The reduction in cohesive strength was originally proposed by for steels by Troiano (25) and furthered by Oriani (28). This would occur near the grain boundaries due to the higher hydrogen concentration enhancing plasticity in the grain boundary region (29),(30). The ability for hydrogen to fracture slip planes is also consistent with the planar transgranular fracture facets observed in the hydrogen-charged 15%-chromium alloy.

The embrittlement observed in these alloys due to hydrogen is similar to the effect observed in hydrogenated water at 54°C (5). The fracture surface morphology of the hydrogen charged high-Cr alloys were very similar to the fracture surfaces observed in the low-temperature fracture-toughness tests performed on Alloy 690 (30% Cr) in hydrogenated water as reported by Brown and Mills (5). The fracture morphology in this work and in results of Brown and Mills (5) showed a change from ductile dimple failure when tested in air to intergranular failure when tested in either the hydrogen charged condition or in 54°C hydrogenated water. Also, the fracture surfaces of the hydrogen-charged low-Cr alloys were very similar to the fracture surfaces observed in the fracture toughness tests performed on Alloy 600 (15% Cr) in low-temperature hydrogenated water. In this case the fracture morphology remained transgranular with some transgranular faceted fracture.

Since the change in fracture surface morphology is the same for both the hydrogen charged condition and the low-temperature hydrogenated-water condition are the same, it is expected that the cause for the embrittlement is the same, hydrogen embrittlement.

CONCLUSIONS

1) Increasing the chromium content increased the ductility of the noncharged Ni-XCr-8Fe alloys. The transgranular failure was replaced by a mixed transgranular/intergranular failure as the chromium concentration increased. The transgranular failure was due to voids nucleating at the primary carbides. It is proposed that the failure strain was increased in the high-chromium alloys due to increased adhesion between the primary carbides and the matrix. The increased failure strain allowed a second failure mechanism to become active, the intergranular failure.

2. Hydrogen only slightly embrittled the low Cr alloys whereas the high Cr alloys showed a marked decrease in ductility with increasing hydrogen content. The intergranular regions in the hydrogen charged specimens were much more brittle appearing than the ductile intergranular fracture observed in the noncharged specimens. It is hypothesized that the decrease in ductility due to the hydrogen was more pronounced in the high Cr alloys due to the increased planarity of slip in these alloys. The failure mode was slip band fracture where the role of hydrogen may have been to decrease the bonding on the slip planes allowing for fracture.

Slip mode played an important role in the hydrogen embrittlement of these alloys, but only a secondary role in the ductility of the noncharged specimens.

3. The fracture surfaces of the hydrogen-charged specimens reported herein and the fracture toughness specimens tested in low-temperature hydrogenated water are very similar. The effect of Cr content on the fracture behavior in water and on hydrogen charged specimens is also similar. This work supports past suggestions that the mechanism of low-temperature SCC in hydrogenated water is hydrogen embrittlement.

ACKNOWLEDGMENTS

This work was supported under U. S. DOE Contract DE-AC-93PN38195 with Bettis Laboratory. The author would like to thank Drs. W. J. Mills, R. Bajaj, and M. G. Burke for many insightful conversations.

REFERENCES

(1) J. P. Foster, W. H. Bamford, R. J. Panthania, "Initial Results of Alloy 600 Crack Growth Rate Testing in a PWR Environment," in Seventh International Symposium on Environmental Degradation of Materials in Nuclear Power Systems-Water Reactors, NACE, Aug. 1995, pp. 25-40

(2) G. L. Webb, "Environamental Degradation of Alloy 600 and Welded Filler Metal EN82 In an Elevated Temoerature Aqueous Environament," in Sixth International Symposium on Environmental Degradation of Materials in Nuclear Power Systems-Water Reactors, Ed. Gold and Simonen, TMS, 1993, pp. 687-695

(3) M. O. Speidel and R. Magdowski, "Stress Corrosion Cracking of Nickel-Base Alloys in High Temperature Water," in Sixth International Symposium on Environmental Degradation of Materials in Nuclear Power Systems-Water Reactors, Ed. Gold and Simonen, TMS, 1993, pp. 361-371

(4) K. Norring, J. Engstrom, P. Norberg, "Intergranular Stress Corrosion Cracking In Steam Generator Tubing, Testing of Alloy 690 and Alloy 600 Tubes," Third International Symposium on Environmental Degradation of Materials in Nuclear Power Systems-Water Reactors, Ed.Theus and Weeks, 1988, pp. 587-593

(5) C. M. Brown and W. J. Mills, "Fracture Toughness, Tensile, and Stress Corrosion Cracking Properties of Alloy 600, Alloy 690, and Their Welds in Water,"Paper #90, Corrosion 96, NACE

(6) C. A. Grove and L. D. Petzold, Corrosion of Nickel-Base Alloys, (ASM, Mars, PA, 1985) pp. 165-180

(7) C. K. Elliott, "Effect of Thermal Treatment on the Fracture Properties of Alloy X-750 in Aqueous Environments," Ph.D. Thesis, Massachusetts Institute of Technology, 1985

(8) A. W. Thompson and I. M. Bernstein, "The Role of Metallurgical Variables in Hydrogen Assisted Environmental Fracture," in Advances in Corrosion Science and Technology, Vol. 7, Eds. M. G. Fontana and R. W. Staehle, Plenum Publishing, 1980

(9) D. M. Symons, Ph.D. Dissertation, Carnegie Mellon University, Pittsburgh, PA, November 1994

(10) B. E. P. Beeston and L. K. France, "Some Stacking-Fault Energies of Some Binary Nickel Alloys Fundamental to the Nimonic Series," J. Inst. Metals, 96, 1968, pp. 105-107

(11) A. W. Thompson, "Hydrogen Assisted Fracture in Single-Phase Nickel Alloys," Scripta Met.,16, 1982, pp. 1189-1192

(12) P. C. J. Gallagher, "The Influence of Alloying, Temperature, and Related Effects on Stacking-Fault Energy," Met. Trans.,Vol.1,1970, pp.2429-2461

(13) J. Crank, Mathematics of Diffusion, Oxford at the Claredon Press, 1956

(14) N. Kishimoto, T. Tanabe, T. Suzuki and H. Yoshida, "Hydrogen Diffusion and Solution at High Temperatures in 316 Stainless Steel, and Nickel-Base Heat-Resistant Alloys,"J. Nuc Mater, Vol. 127, 1985, pp.1-9

(15) R. C. Scarberry, S. C. Pearlman, J. R. Crum, "Precipitation Reactions in Inconel 600 and Their Effects on corrosion Behavior," Corrosion, 32, 1976, pp. 401-406

(16) J. J. Kai, and M. N. Liu, "The Effects of heat Treatment on the Carbide Evolution and the Chromium Depletion Along Grain Boundaries of Inconel 690 Alloy, "Scripta Met., 23, 1989, pp. 17-22

(17) P. S. Kotval, "Carbide Precipitation on Imperfections in Superalloy Matrices," Trans. AIME, Vol. 242, 1968, 1651-1656

(18) N. Clement, D. Caillard, J. L. Martin, " Heterogeneous deformation of Concentrated Ni-Cr FCC Alloys: Macroscopic and Microscopic Behavior," Acta Met, Vol. 1342, No. 6, 1984, 961-975

(19) J. E. Franklin, G. Judd, and G. S. Ansell, Proc. 3rd ICSMA, Iron and Steel Institute, London, Vol. 1, 1973, p. 345

(20) G. H. Gessinger, H. F. Fischmeister, and H.L. Lukas, Powder Metall. 16(31), 1973, p. 119

(21) E. E. Stansbury, C. R. Brooks, and T. L. Arledge, "Specific-Heat Anomolies in Solid Solutions of Chromium and Molybdenum in Nickel:Evidence fo(24)r Short-Range Order," J. Inst. Metals, Vol. 94, 1966, pp. 136-138

(22) A. Akhtar and E. Teghtsoonian, "Plastic deformation of Ni-Cr Single Crystals," Met. Trans., Vol 2, 1971, pp. 2757-2763

(23) K. Miyata and M. Igarashi, "Effect of Ordering on Susceptibility to Hydrogen Embrittlement of a Ni-Base Superalloy," Met. Trans. A, 1992, p. 953-961

(24) D. L. Douglass, G. Thomas, W. R. Roser, "Ordering, Stacking Faults, and Stress Corrosion Cracking," Corrosion, Vol. 20, 1964, pp. 15t-28t

(25) E. A. Steigerwald, F. W. Schaller and A. R. Troiano, Trans. AIME, 218, 1960, p. 832-841

(26) W. M. Garrison and N. R. Moody,"Ductile Fracture," J. Phys. Chem. Solids, Vol. 48, No. 11, 1987, pp. 1035-1074

(27) S.V. Nair, R.R. Jensen, J.K. Tien, Metall. Trans.,Vol.14A,1983, pp.385-393

(28) R. A. Oriani and P. H. Josephic, Acta Metall., 22, 1974, p. 1065-1074

(29) J. Eastman, T. Matsumoto, N. Narita, F. Heubaum, and H. K. Birnbaum, in Hydrogen Effects in Metals, Eds. A. W. Thompson and I. M. Bernstein, (Warrendale, PA), 1986, pp. 397-409

(30) I. M. Robertson and H. K. Birnbaum, Acta Metall., 34, 1986, p. 353-366

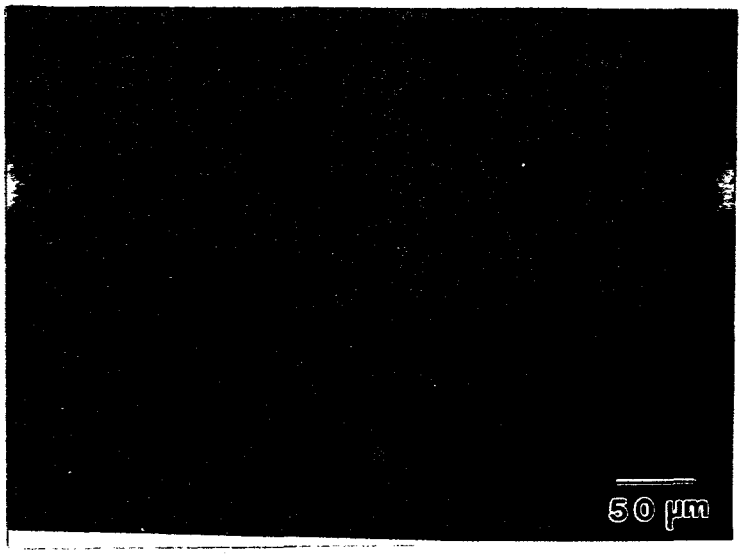

Figure 1: Light Optical Micrographs of Alloy 1(6% Cr)

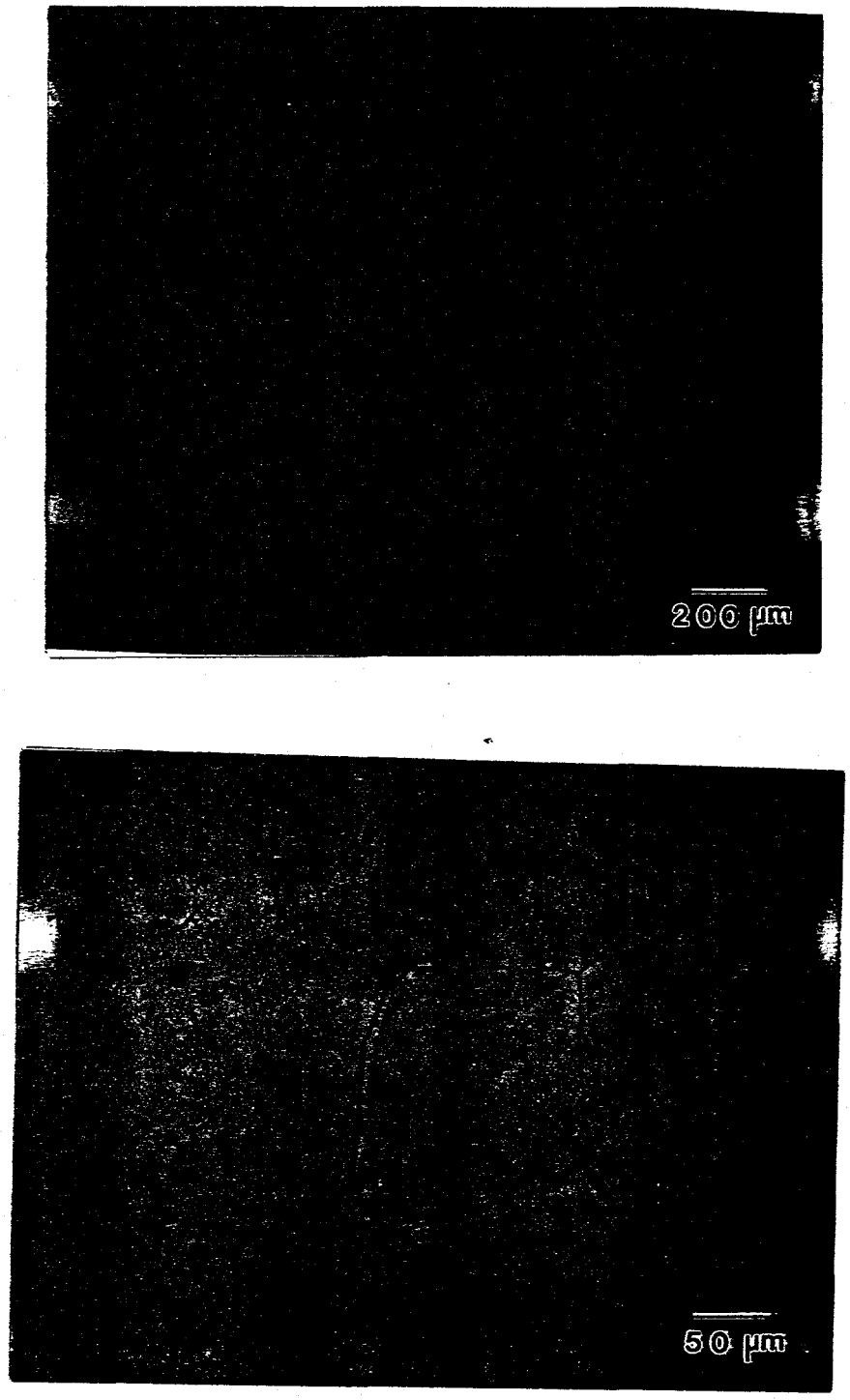

Figure 2: Light Optical Microsgraphs of Alloy 2 (15% Cr)

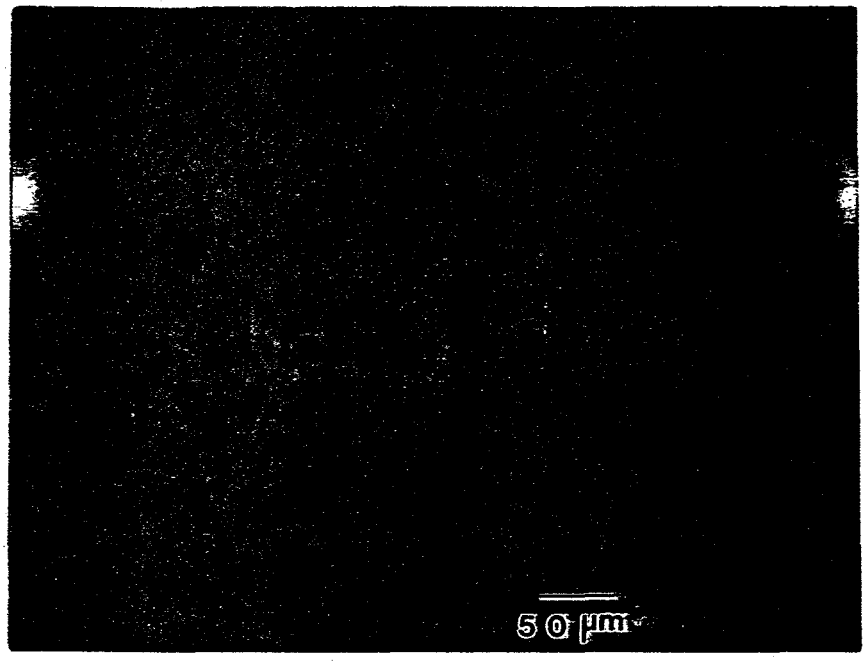

Figure 3: Light Optical Micrographs of Alloy 3 (26% Cr)

Figure 4: Light Optical Micrographs of Alloy 4 (35% Cr)

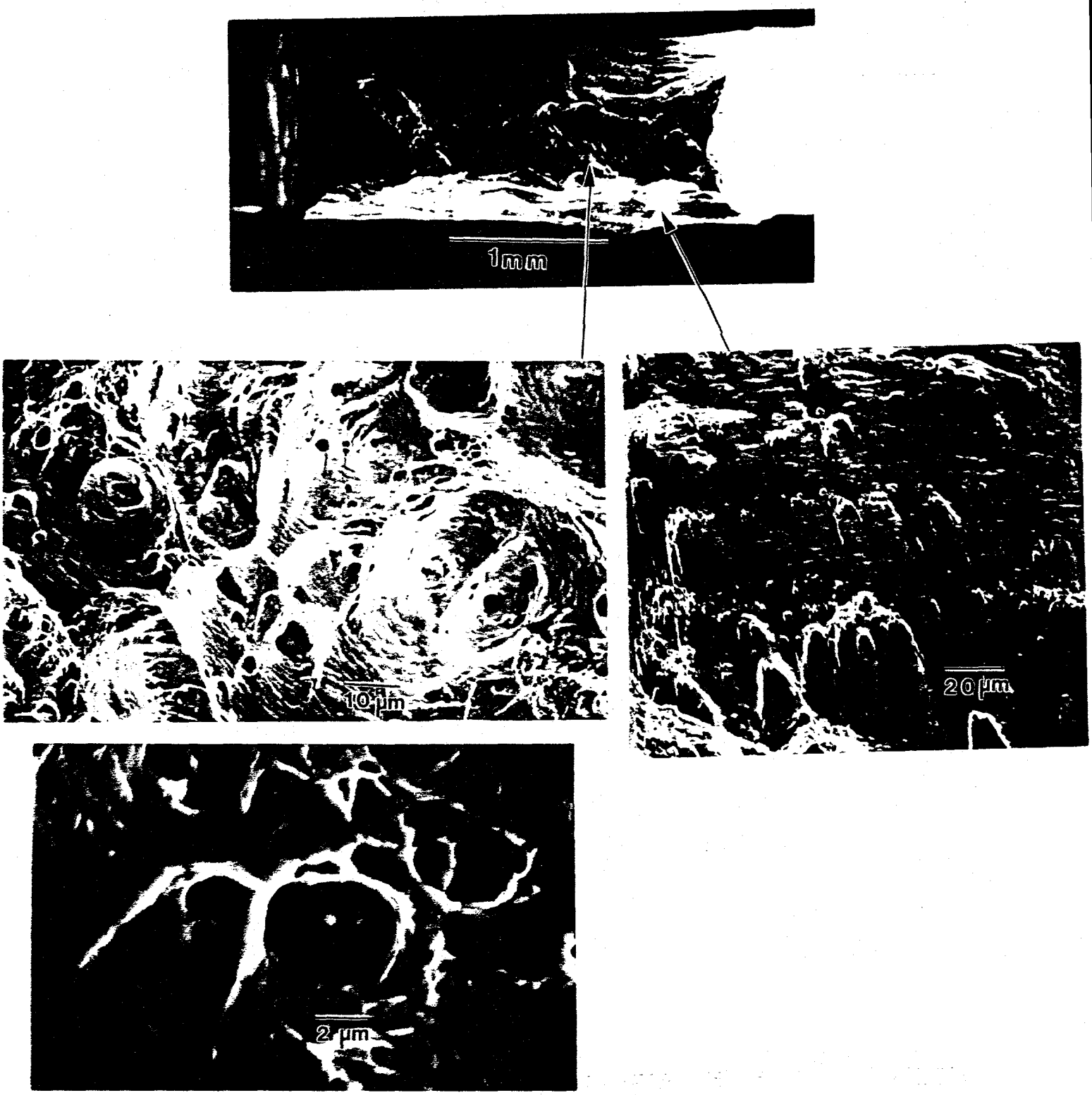

Figure 5: SEM Fractographs of Noncharged Tensile Specimen of

Alloy 1(6% Cr) showing the Ductile Failure Modes

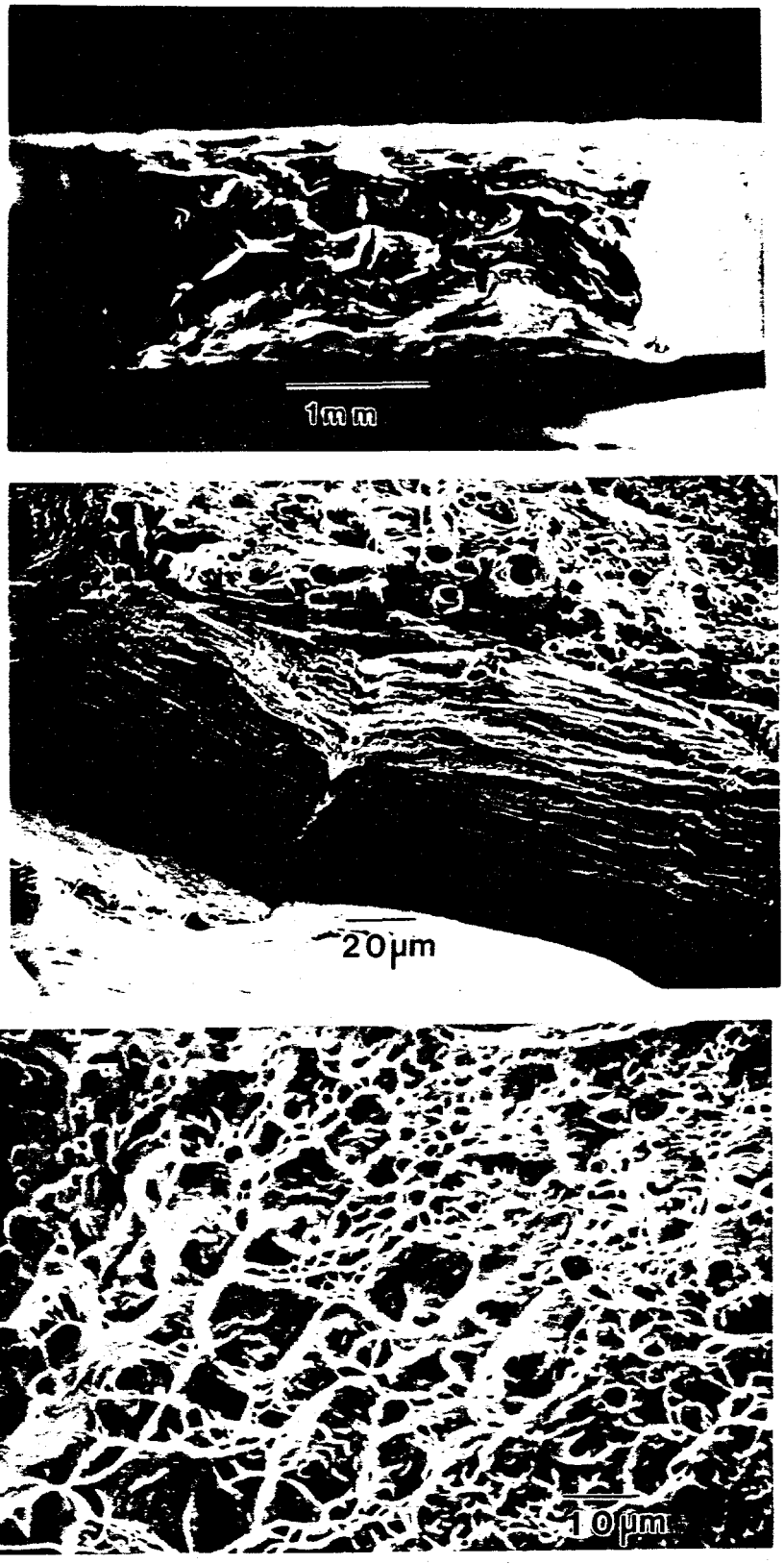

Figure 6: SEM Fractorgraphs of Noncharged Tensile Specimen of Alloy 4 (35% Cr)

Showing the transgranular dimples and the intergranular tearing

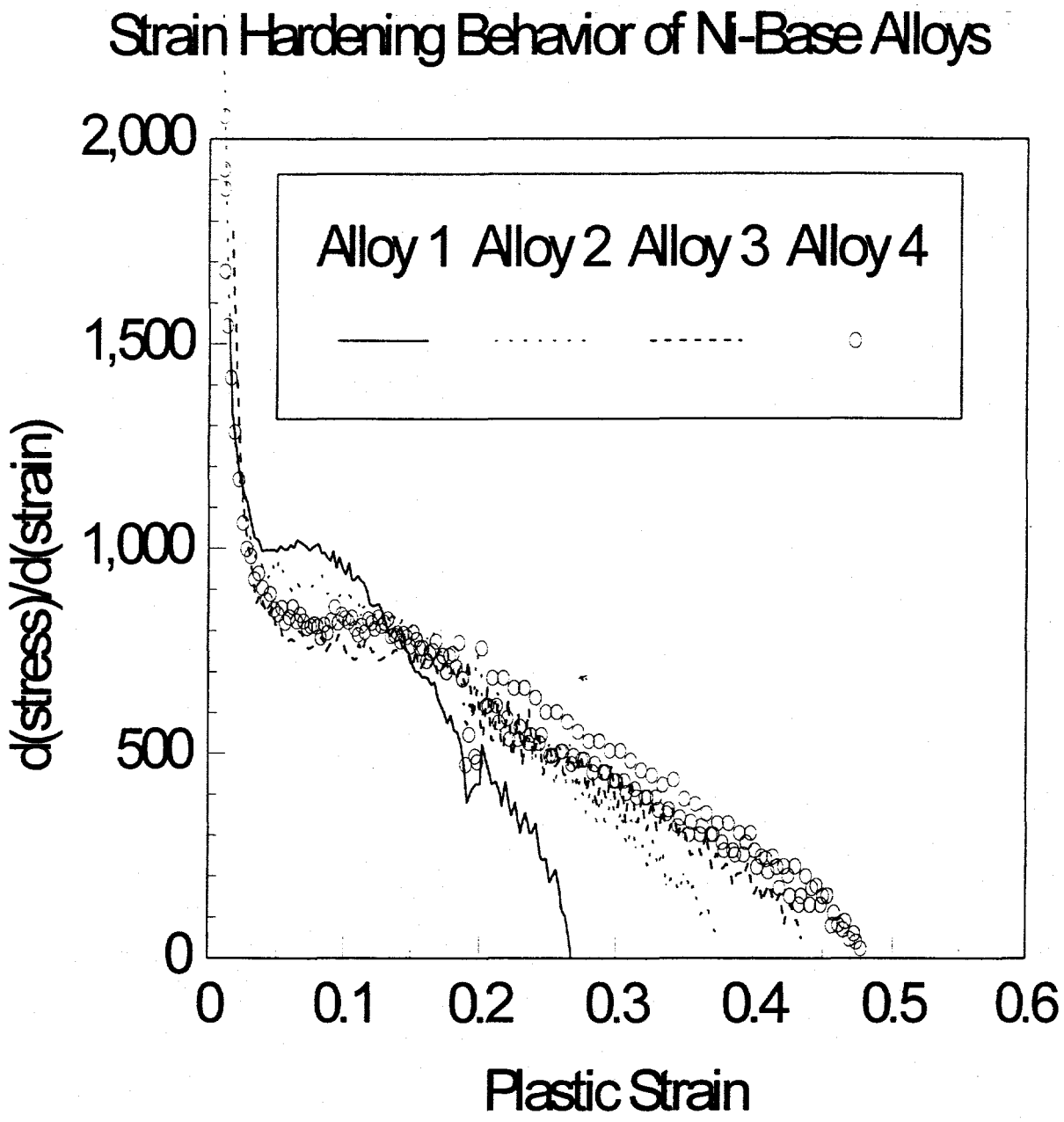

Figure 7:The Strain Hardening Behavior of Alloys 1 through 4

(Alloy 1: 6% Cr, Alloy 2: 15% Cr, Alloy 3: 25% Cr, Alloy 4:35%Cr)

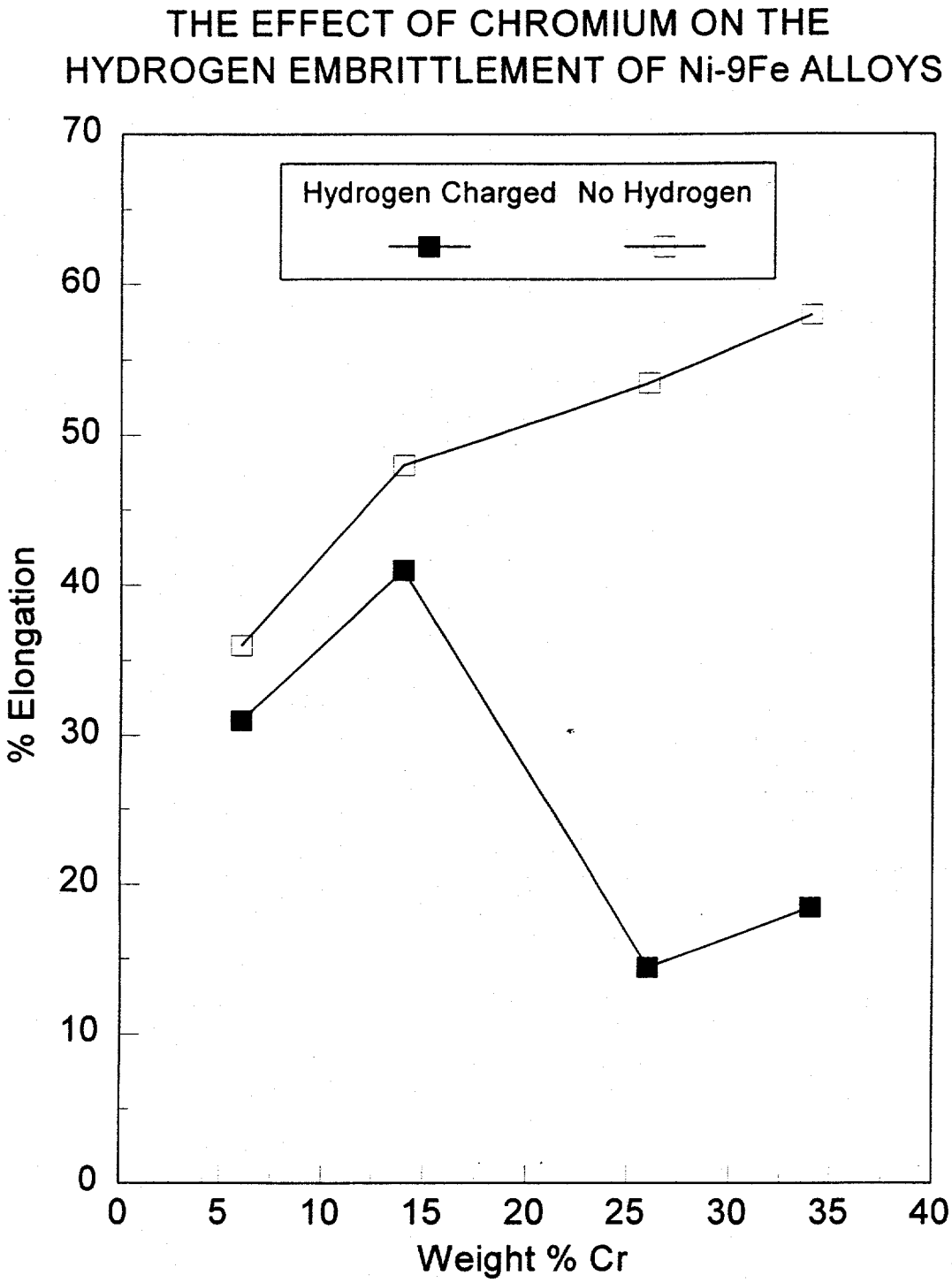

Figure 8: The Effect of Cr on the Ductility of

Hydrogen-Charged and Noncharged Tensile Specimens

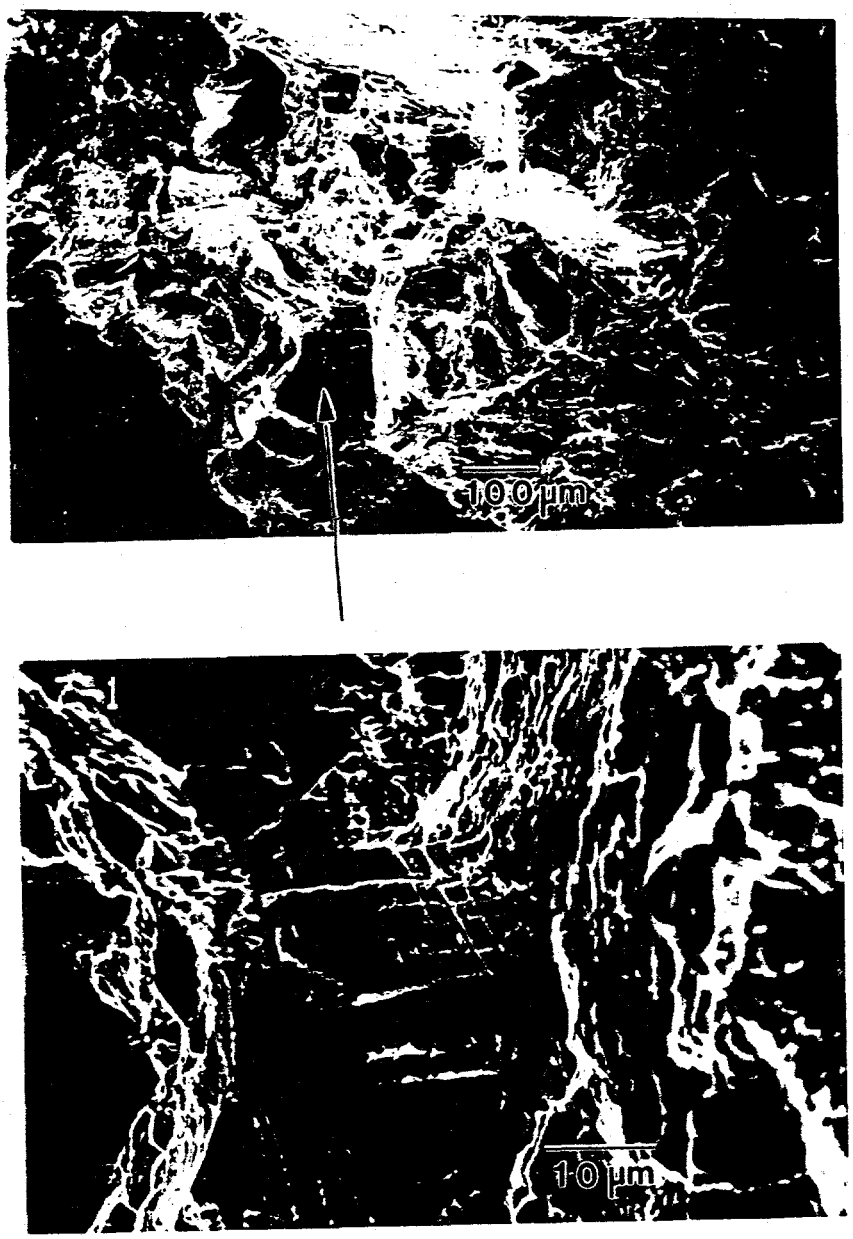

Figure 9: SEM Fractographs of Hydrogen-Charged Specimen of Alloy 2 (14%Cr)

Showing Area of Transgranular Faceted Fracture

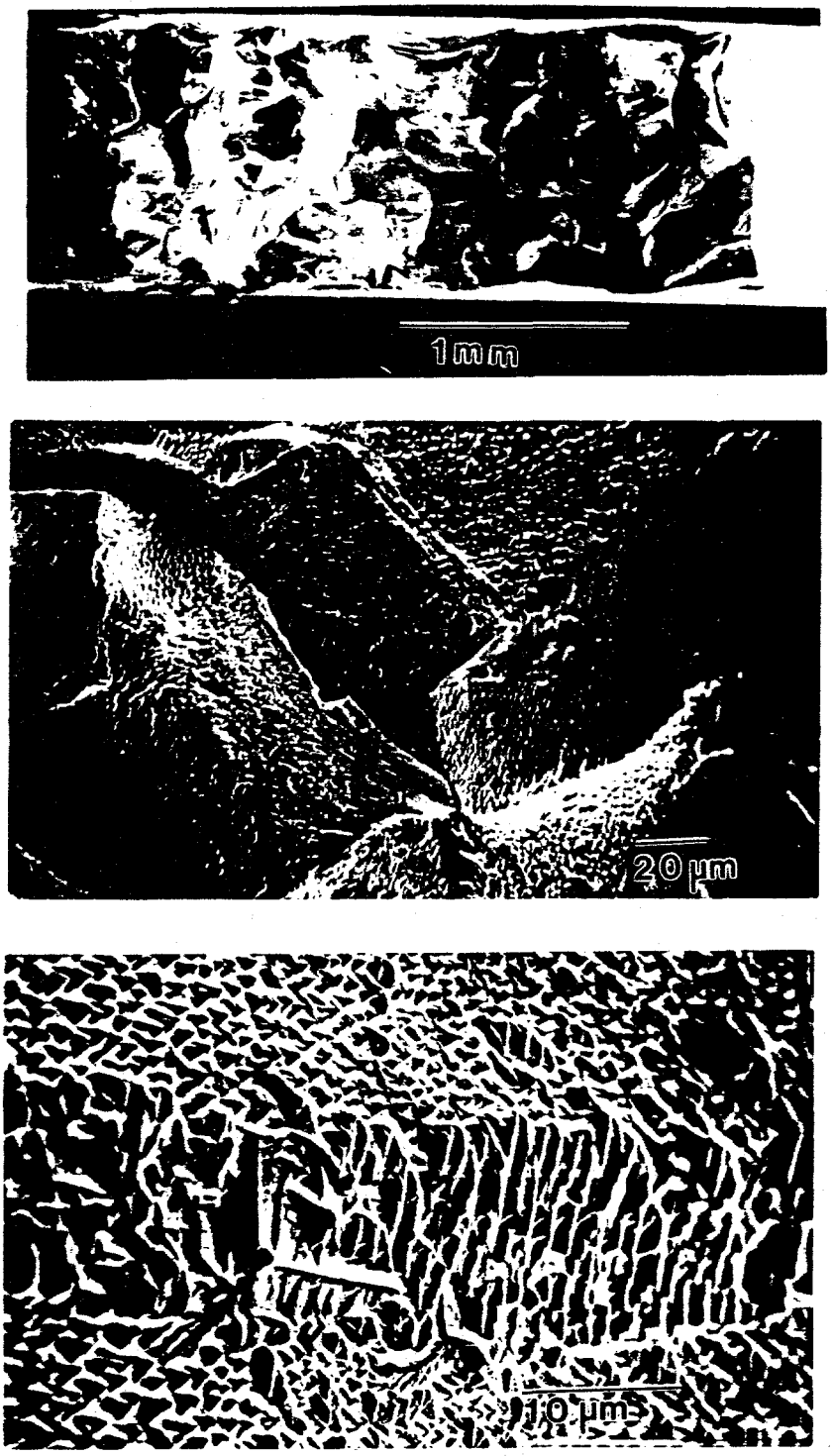

Figure 10: Fractography of Hydrogen-Charged Specimen of Alloy 4 (35% Cr) Showing Faceted Intergranular Fracture

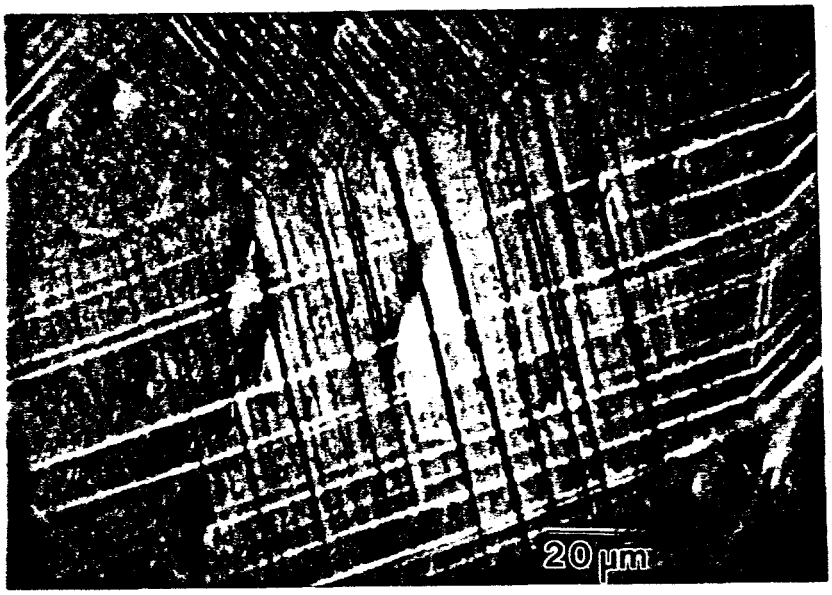

Figure 11: Slip Lines Observed on a Polished Uniaxial Tensile Specimen of Alloy 9 (35% Cr)

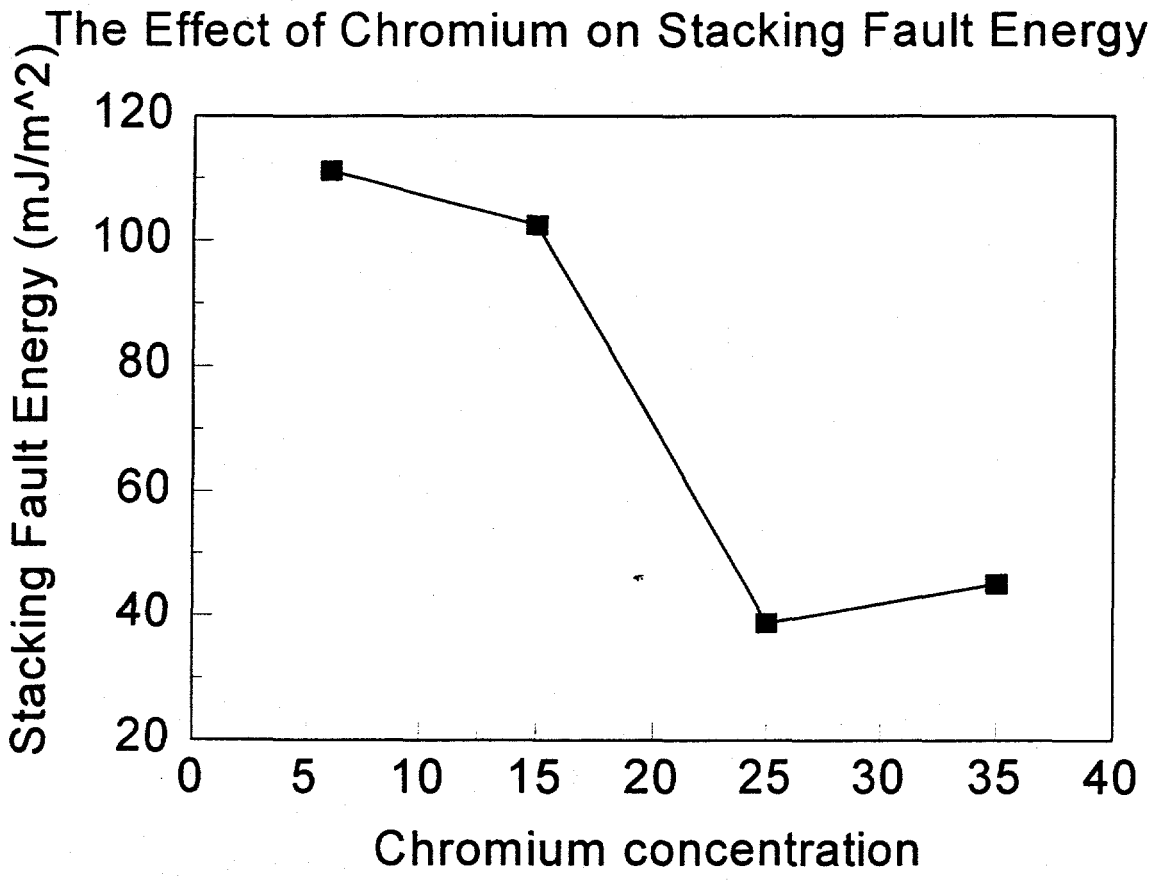

Note Fe was not incorporated into SFE calculation

Figure 12: Effect of Cr Concentration on the Stacking Fault Energy of Ni-Cr Alloys

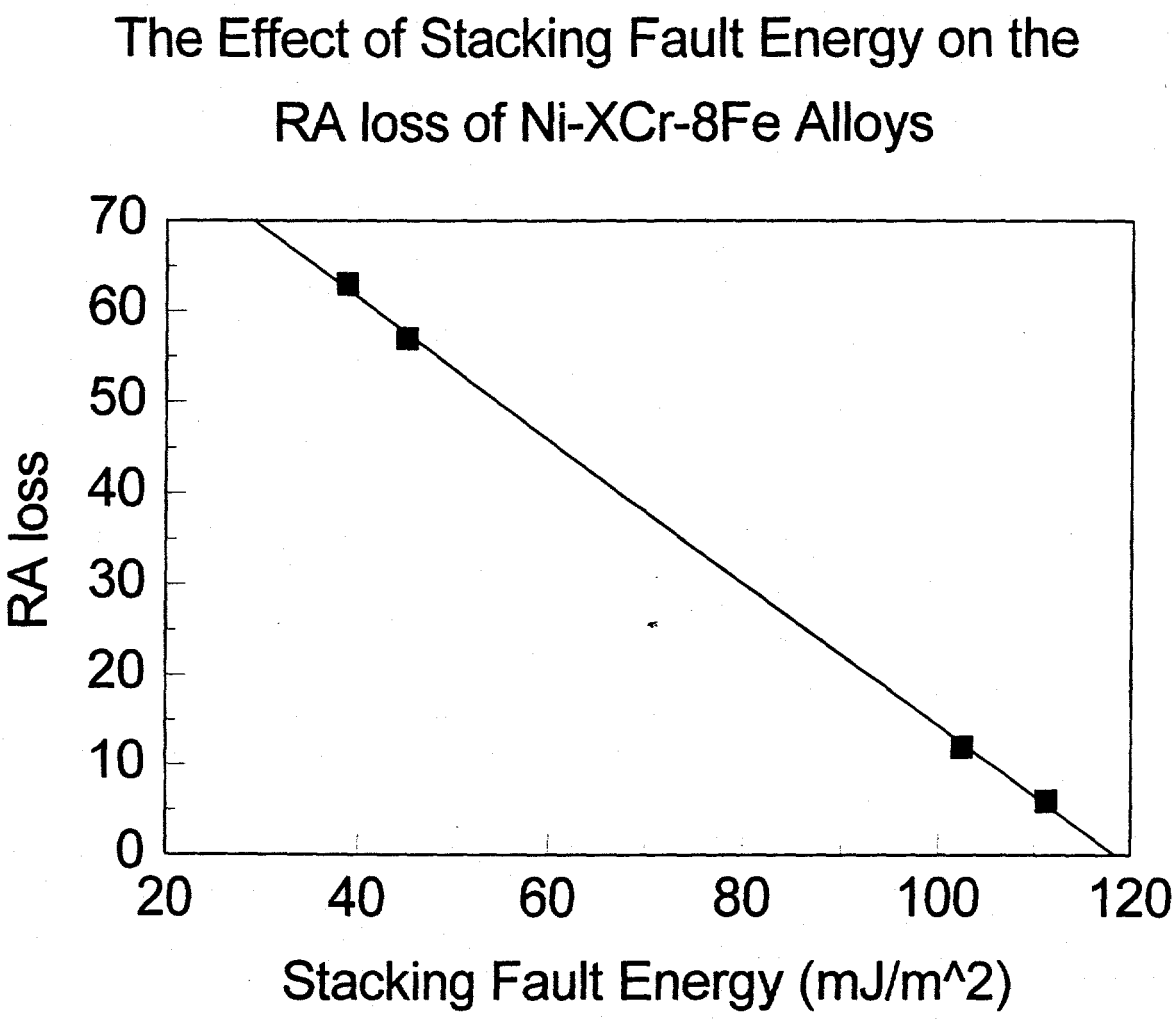

Note Fe was not incorporated into SFE calculation

Figure 13: Effect of Stacking Fault Energy on the Embrittlement of Ni-XCr-8Fe Alloys